

Millimeter-Wave E-Plane Waveguide Bandpass Filters Based on Spoof Surface Plasmon Polaritons

Yiqun Liu¹, *Student Member, IEEE*, Kai-Da Xu¹, *Senior Member, IEEE*, Jianxing Li¹, *Member, IEEE*,
Ying-Jiang Guo¹, *Member, IEEE*, Anxue Zhang¹, *Member, IEEE*,
and Qiang Chen¹, *Senior Member, IEEE*

Abstract—A class of millimeter-wave E-plane waveguide bandpass filters (BPFs) based on spoof surface plasmon polaritons (SSPPs) have been presented in this article. Three kinds of SSPPs, with different patterns coated on the dielectric substrate, are inserted into the E-plane of WR-10 standard rectangular waveguide for the design of BPFs. To clarify the filtering characteristics of the proposed BPFs, the dispersive properties of different SSPP unit cells are investigated and discussed. The electromagnetic simulation results demonstrate that the bandwidths and center frequencies of the proposed E-plane waveguide BPFs can be flexibly adjusted by controlling the asymptotic frequencies of SSPP unit cells. For verifying the design feasibility, these three E-plane waveguide BPFs are fabricated and measured. Good agreement between measurements and simulations indicates that the proposed idea will be a good candidate for the BPF design with low insertion loss and flexible adjustment of center frequency and bandwidth.

Index Terms—Bandpass filter (BPF), dispersive characteristics, E-plane waveguide, millimeter wave, spoof surface plasmon polaritons (SSPPs).

I. INTRODUCTION

IN THE past few decades, the unavoidable tension of frequency spectrum resources increases the working frequency of a wireless communication system from low-frequency band to millimeter-wave band. The millimeter-wave bands, e.g., W-band, with merits of wide bandwidth, large capacity, and high resolution, are attracting more and more attention for

the applications of millimeter-wave imaging, automotive anti-collision radar [1], [2], [3], and so on. As one of the key components in the wireless communication systems, a millimeter-wave bandpass filter (BPF) with high performance is extensively required to meet the industrial application. However, few design technologies of millimeter-wave BPFs can successfully balance the fabrication cost and filtering performance, such as low in-band loss and high selectivity.

So far, numerous millimeter-wave BPFs based on various technologies have been reported [4], [5], [6], [7], [8], [9], [10], [11], [12], [13], [14], [15]. Among them, the SiGe/GaAs/silicon-based millimeter-wave BPFs [4], [5], [6], [7], [8] have undeniably small sizes, which can be naturally integrated with on-chip radio frequency circuits and front ends for the miniaturization of wireless communication systems. Especially, the commercial silicon-based CMOS technologies are very mature, resulting in massive productions of critical devices, including light-emitting devices [16], [17], [18], [19]. However, the practical applications of semiconductor-based BPFs generally suffer from the issues of high fabrication cost and large insertion losses. On the other hand, the substrate integrated waveguide (SIW) technology was employed for the design of millimeter-wave BPFs [9], [10], [11], [12], which could be fabricated on commercial single-layer or multilayer printed circuit board (PCB) with low cost. Moreover, some millimeter-wave BPFs based on low-temperature cofired ceramic (LTCC) technology were reported to realize the miniaturized sizes [13], [14], [15]. Unfortunately, the multilayer filter structure design was complicated, and the fabrication cost was also relatively high.

The E-plane waveguide BPF, as one of the feasible filter solutions for the millimeter-wave transmitter/receiver systems, has been further explored recently [20], [21], [22], due to the flexibly adjusted ability through changing the resonant topology on the inserted substrate. For instance, a W-band E-plane waveguide BPF is proposed in [20], whose transmission zeros (TZs) at upper and lower stopbands can be controlled by a meander ring resonator and two metallic strips. In [21], the bandwidth and center frequency of E-plane waveguide BPF can be tuned by adjusting the geometric parameters of strip lines and L-shaped resonators.

Manuscript received 23 June 2022; accepted 9 July 2022. Date of publication 17 August 2022; date of current version 5 October 2022. This work was supported in part by the NSAF Joint Fund under Grant U2130102, in part by the Fundamental Research Funds of Shaanxi Key Laboratory of Artificially Structured Functional Materials and Devices under Grant AFMD-KFJJ-21104, in part by the State Key Laboratory of Advanced Optical Communication Systems Networks under Grant 2022GZKF020, and in part by the Siyuan Scholar Fellowship of Xi'an Jiaotong University (XJTU). (Yiqun Liu and Kai-Da Xu contributed equally to this work.) (Corresponding author: Kai-Da Xu.)

Yiqun Liu, Kai-Da Xu, Jianxing Li, and Anxue Zhang are with the School of Information and Communications Engineering, Xi'an Jiaotong University, Xi'an 710049, China (e-mail: kaidaxu@ieee.org).

Ying-Jiang Guo is with Allwinner Technology Company Ltd., Zhuhai 519000, China.

Qiang Chen is with the Department of Communications Engineering, Graduate School of Engineering, Tohoku University, Sendai 980-8579, Japan.

Color versions of one or more figures in this article are available at <https://doi.org/10.1109/TMTT.2022.3197593>.

Digital Object Identifier 10.1109/TMTT.2022.3197593

0018-9480 © 2022 IEEE. Personal use is permitted, but republication/redistribution requires IEEE permission.
See <https://www.ieee.org/publications/rights/index.html> for more information.

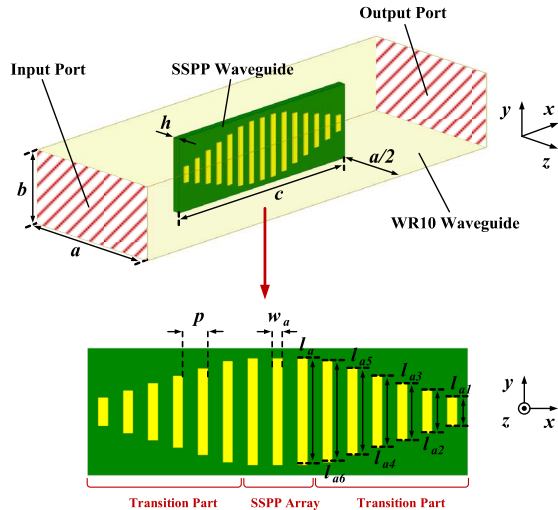


Fig. 1. Millimeter-wave E-plane waveguide BPF based on uniform SSPPs.

Surface plasmon polaritons (SPPs) are highly confined surface waves propagating along the interface between the metal and the dielectric at optical frequency [23]. As a kind of periodic metamaterials supporting the SPPs-like surface wave at microwave band [24], spoof SPPs (SSPPs) possess the advantages of strong confinement ability of electromagnetic wave and excellent low-pass transmission characteristics [25]. Therefore, the SSPPs have been applied in many designs of planar microwave and millimeter-wave devices [26], [27], [28], [29], [30], [31], [32], [33], [34], [35]. To the best of the authors' knowledge, however, very little exploration has been done on the design of millimeter-wave E-plane waveguide BPF based on SSPPs. In this article, based on our previous work [36], three different but very simple structures of SSPPs are presented and applied in the millimeter-wave E-plane waveguide BPFs. By controlling the asymptotic frequencies of SSPPs, the bandwidths and center frequencies of millimeter-wave E-plane waveguide BPFs can be flexibly adjusted. Good agreement between simulated and measured results of the fabricated examples validates the design feasibility.

II. CHARACTERISTICS OF E-PLANE WAVEGUIDE BPF BASED ON SSPPS

A millimeter-wave E-plane waveguide BPF based on uniform SSPPs is proposed in Fig. 1, where the SSPPs metallic structures are coated on an FSD220G substrate (thickness $h = 0.127$ mm, relative permittivity $\epsilon_r = 2.2$, and loss tangent $\delta = 0.009$). As illustrated in Fig. 1, a pair of gradient transition parts from rectangular waveguide to SSPPs are designed for the excitation of SSPP mode in millimeter-wave E-plane waveguide BPF. All dimensions of the proposed BPF are tabulated in Table I.

The dispersive characteristics of the uniform SSPP unit cell shown in Fig. 2(a) (inset) are investigated and discussed. Fig. 2(a)–(c) displays the dispersion curves of uniform SSPP unit cell with different values of l_a , p , and w_a , respectively. It can be found that the variations of l_a and p have more obvious effects on the change of asymptotic

TABLE I
DIMENSIONS OF MILLIMETER-WAVE E-PLANE WAVEGUIDE BPF (UNIT: mm)

Parameter	l_a	l_{a1}	l_{a2}	l_{a3}	l_{a4}
Value	1.07	0.28	0.426	0.572	0.718
Parameter	l_{a5}	l_{a6}	p	w_a	a
Value	0.864	1.01	0.25	0.1	2.54
Parameter	b	c	h		
Value	1.27	3.81	0.127		

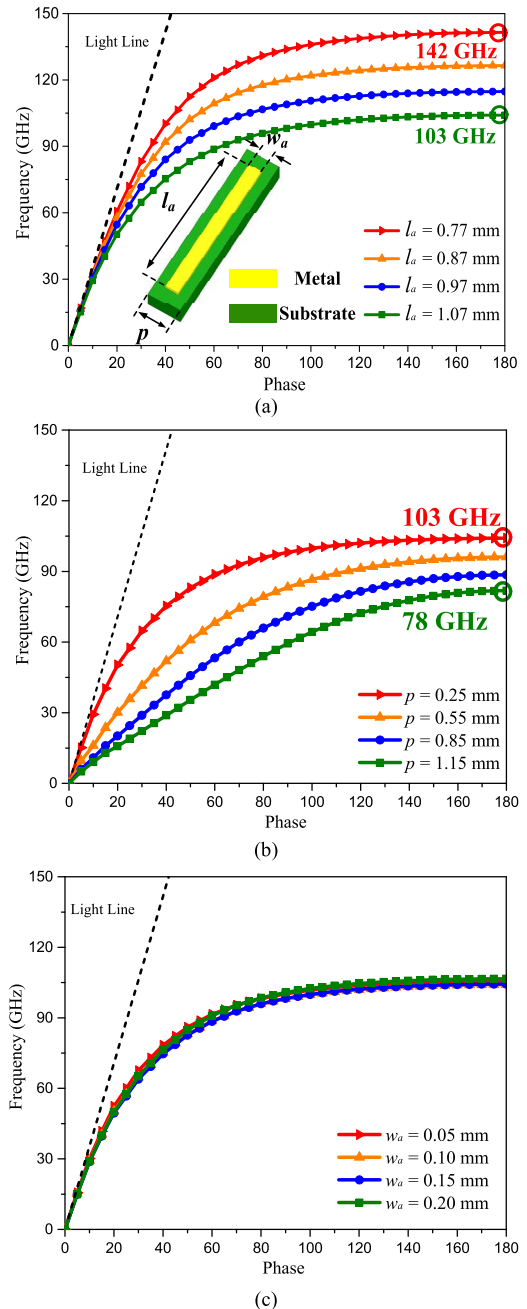


Fig. 2. Dispersion curves of uniform SSPP unit cell with different values of (a) l_a , (b) p , and (c) w_a .

frequency than that of w_a . The asymptotic frequency can be effectively adjusted from 142 to 103 GHz with an increase

of l_a from 0.77 to 1.07 mm in Fig. 2(a). As p increases from 0.25 to 1.15 mm in Fig. 2(b), the asymptotic frequency is decreased from 103 to 78 GHz. However, larger p will obviously decrease the slopes of dispersion curves near the asymptotic frequency points, which implies that the uniform SSPPs will have weaker confinement ability of electric field, and the design of waveguide BPF with sharp roll-off skirt will be difficult. Besides, the increase of p will unavoidably extend the size of SSPP waveguide in the x -direction, which is not friendly for the compact design of SSPP waveguide. Therefore, the parameter l_a seems to be a better option for the design and adjustment of millimeter-wave E-plane waveguide BPF than the other two parameters.

To achieve the mode and impedance matching for the proposed BPF, a kind of gradient transition parts at the input–output (I/O) ports is designed on SSPP waveguide. The y -directional lengths of metallic strips of gradient transition parts are set as

$$l_{an} = 0.146(n - 1) + 0.28, \quad n = 1, 2, \dots, 6 \quad (1)$$

where the unit is mm. Under the mathematical conditions that $\lambda \gg p$ and $\lambda \gg l$ (λ denotes the operating wavelength, and l represents the length of metallic strip in the y -direction), the wavenumber k_x can be expressed as the following [24], [25]:

$$k_x = k_o \sqrt{1 + \frac{(p - w_a)^2}{(p)^2} \tan^2(k_o l / 2)} \quad (2)$$

where k_o and k_x denote the wavenumbers in free space and SSPP waveguide, respectively. The structures of E-plane waveguide BPFs with and without gradient transition parts are presented in Fig. 3(a) (inset). Fig. 3(a) shows the calculated wavenumber k_x at 80 GHz, which is the center frequency of the proposed BPF. For the case of BPF without gradient transition parts, it can be observed that a mismatch of wavenumber exists between the WR-10 rectangular waveguide and the SSPP waveguide, in which the wavenumber k_x jumped from k_o to $1.25k_o$ directly. On the contrary, the wavenumber k_x can be gradually changed from k_o to $1.25k_o$ for the BPF with gradient transition parts.

For demonstrating the function of gradient transition parts, the S-parameters of BPF with and without gradient transition parts are simulated, respectively, as illustrated in Fig. 3(b). If the gradient transition parts are not applied, the value of $|S_{11}|$ of the proposed BPF is close to -3 dB in the whole passband, which means nearly half power of the electromagnetic waves is reflected. In contrast, a high-efficiency transmission within the passband can be achieved for the BPF with gradient transition parts, in which $|S_{11}|$ is lower than -10 dB, and $|S_{21}|$ is flat from 63 to 103 GHz.

To observe the mode conversion of electromagnetic waves of gradient transition parts, the electric field distributions of the proposed millimeter-wave E-plane waveguide BPF are simulated at 80 GHz. The top view of electric field distribution of the proposed BPF is displayed in Fig. 4(a). The electric field distributions of y - o - z cross section at the outside, fourth metallic strip, and eighth metallic strip of SSPP waveguide are presented in Fig. 4(b)–(d), respectively. Moreover, the electric

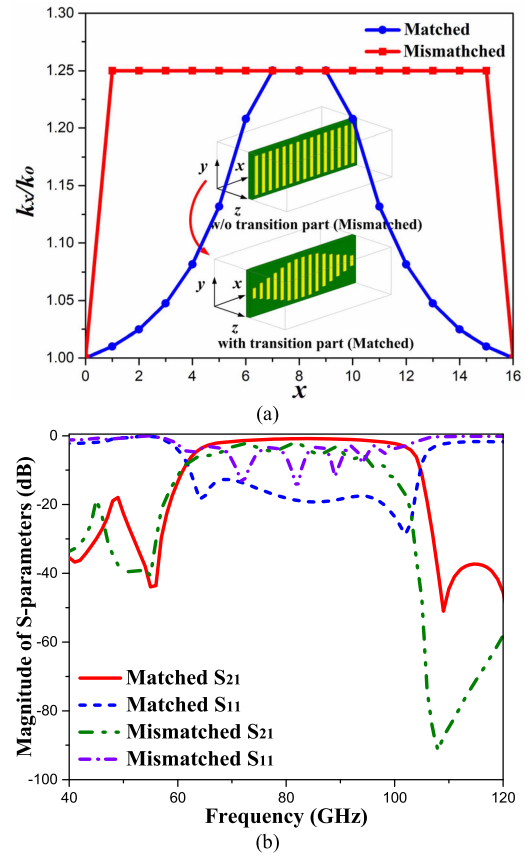


Fig. 3. (a) Wavenumber k_x of SSPP waveguide with and without gradient transition parts and (b) simulated S-parameters of E-plane waveguide BPF based on uniform SSPPs with and without gradient transition parts.

field intensities of Fig. 4(c) and (d) are displayed in Fig. 4(e) and (f) for easier observation. The distribution of electric field $|E|$ of Fig. 4(e) and (f) along the y -axis is quantified for clearer comparisons. The observation heights of electric field $|E|$ are set as $z = 0.05$ mm and $z = 0.5$ mm, and the quantified results are displayed in Fig. 5.

As shown in Fig. 4(b)–(d), the electromagnetic waves propagate with the TE_{10} mode along WR-10 rectangular waveguide until they arrive at the outmost metallic strip of the proposed BPF. The color of electric field distributions near the surface of metallic strips in Fig. 4(c) is deeper than that in Fig. 4(d). The areas far away from the eighth metallic strip have less electric field distributions than that of the fourth metallic strip in y - o - z cross section, which is more obvious in Fig. 4(e) and (f). In addition, the magnitude value of electric field $|E|$ of the eighth metallic strip is larger than that of the fourth metallic strip for the case of $z = 0.05$ mm in Fig. 5(a). In contrast, when the observation height is set as $z = 0.5$ mm in Fig. 5(b), the eighth metallic strip has weaker electric field $|E|$ than that of the fourth metallic strip, which is because more electric field is concentrated on the surface of the eighth metallic strip.

Therefore, the propagation of electromagnetic waves can be confined near the surface of SSPP waveguide, and the electromagnetic waves can be smoothly transferred from the TE_{10} mode to surface-wave mode through the proposed gradient transition parts.

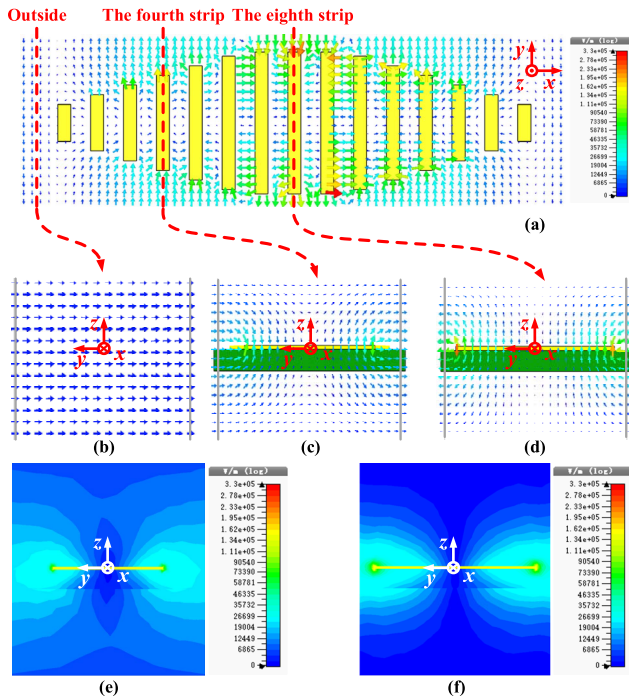


Fig. 4. Electric field distribution of (a) top view of the proposed BPF. Electric field distributions of y - o - z cross section at three different locations, including (b) outside of SSPP waveguide, (c) fourth metallic strip, and (d) eighth metallic strip. Electric field intensities of y - o - z cross section at (e) fourth metallic strip and (f) eighth metallic strip.

Fig. 6(a) displays the simulated S-parameters of the WR-10 waveguide and the proposed millimeter-wave E-plane waveguide BPF based on uniform SSPPs in Ansys HFSS. It can be observed that the simulated 3-dB bandwidth of the proposed BPF is from 63 to 103 GHz with a minimum insertion loss of 0.55 dB at the center frequency of 83 GHz. Since the variation of lower cutoff frequency of the proposed BPF is limited to the fixed WR-10 waveguide, the adjustment of filtering performance mainly depends on the change of upper cutoff frequency, i.e., asymptotic frequency of the uniform SSPP unit cell. As l_a increases from 1.01 to 1.07 mm, the upper cutoff frequency will be reduced from 105 to 103 GHz for the proposed BPF, as shown in Fig. 6(b). Besides, the proposed BPF has a wide out-of-band rejection, whose bandwidths of lower and upper stopbands are 62 and 53 GHz (referring to -10 dB), respectively.

III. E-PLANE WAVEGUIDE BPFs BASED ON DIFFERENT SSPPs STRUCTURES

Although the upper cutoff frequency of the proposed BPF can be widely adjusted from 103 to 142 GHz with a variation of l_a , the maximum available value of l_a for the uniform SSPP unit cell is only 1.07 mm limited by the fabrication resolution and the fixed size (1.27 mm) of WR-10 rectangular waveguide in the y -direction, which makes the minimum upper cutoff frequency of proposed BPF merely as low as 103 GHz. Therefore, it is impossible to further decrease the upper cutoff frequency of the proposed millimeter-wave E-plane waveguide BPF based on uniform SSPPs. To solve the issue,

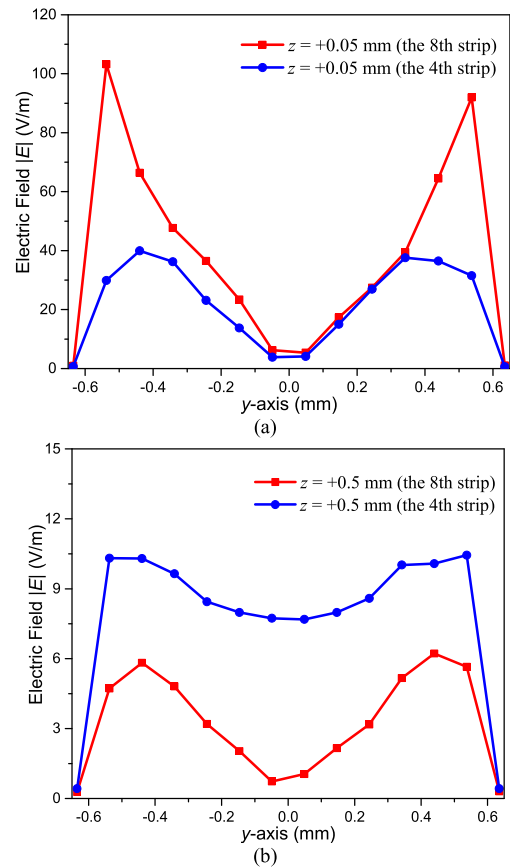


Fig. 5. Distribution of electric field $|E|$ of the fourth and eighth metallic strips along the y -axis at (a) $z = 0.05$ mm and (b) $z = 0.5$ mm.

two different millimeter-wave E-plane waveguide BPFs based on stepped-impedance and grounded SSPPs are proposed and analyzed in this section, respectively.

A. Millimeter-Wave E-Plane Waveguide BPF Based on Stepped-Impedance SSPPs

The structure of the stepped-impedance SSPP unit cell and its initial dimensions are presented in Fig. 7. The dispersion curves of stepped-impedance SSPP unit cell with different parameters w_{b1} and l_n are simulated in CST microwave studio software. Fig. 8 shows the dispersion curves of stepped-impedance SSPP unit cell with different values of w_{b1} . It can be observed that the increase of w_{b1} from 0.1 to 0.16 mm will effectively decrease the asymptotic frequency from 103 to 93 GHz. Table II presents the relationships between the asymptotic frequencies and the lengths of l_n . The asymptotic frequency of the proposed stepped-impedance SSPP unit cell drops to 96 GHz first as the decrease of l_n and then rises again. Both variations of w_{b1} and l_n do not increase the extra size of SSPP waveguide.

Due to a wider adjustment range that can be effectively achieved by changing w_{b1} than that of l_n , parameter w_{b1} is mainly used for the design and optimization of E-plane waveguide BPF. The structure of the proposed millimeter-wave E-plane waveguide BPF based on stepped-impedance SSPPs is displayed in Fig. 9, and its dimensions are tabulated in

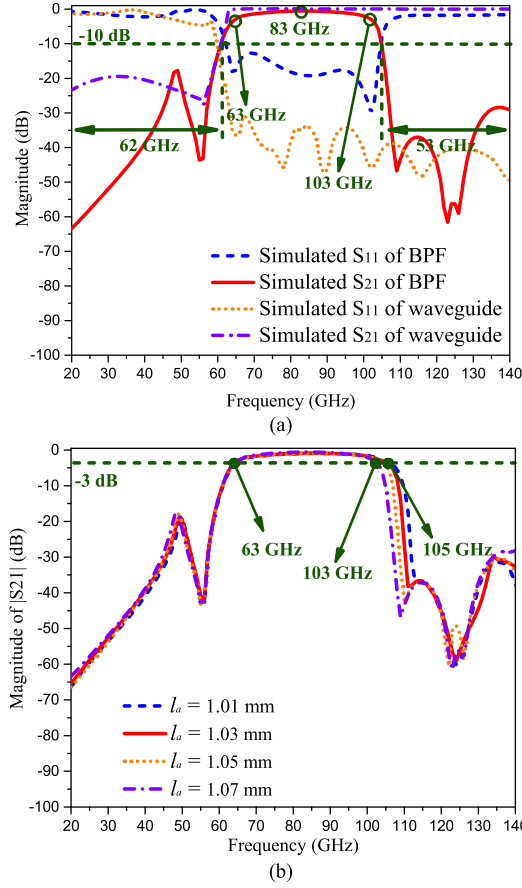


Fig. 6. (a) Simulated S-parameters of WR-10 waveguide and the proposed millimeter-wave E-plane waveguide BPF based on uniform SSPPs and (b) magnitude of $|S_{21}|$ with a variation of l_a for E-plane waveguide BPF based on uniform SSPP unit cell.

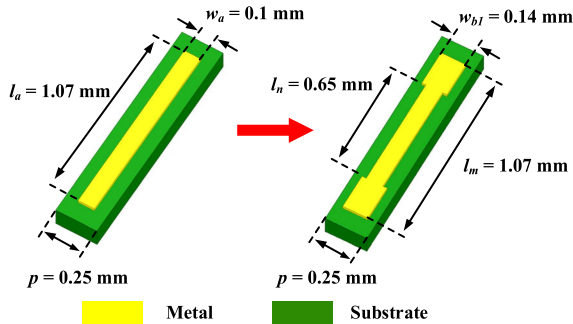


Fig. 7. Structural comparisons of uniform and stepped-impedance SSPP unit cells.

Table III. For this case, the y -directional lengths of metallic strips of gradient transition parts are set as follows:

$$l_{bn} = 0.166(n - 1) + 0.2, \quad n = 1, 2, \dots, 6. \quad (3)$$

The S-parameters of the proposed millimeter-wave E-plane waveguide BPF based on stepped-impedance SSPPs are simulated in Fig. 10(a). It has a flat passband from 65 to 95 GHz with a 3-dB fractional bandwidth of 37.5%, and its simulated center frequency is at 80 GHz with a minimum insertion loss of 0.38 dB. Meanwhile, the proposed BPF has a wide out-of-band rejection (referring to -10 dB), whose simulated

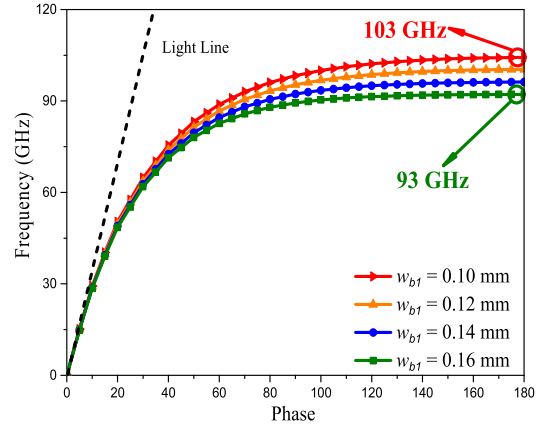


Fig. 8. Dispersion curves of stepped-impedance SSPP unit cell with different values of w_{b1} .

TABLE II
RELATIONSHIPS BETWEEN ASYMPTOTIC FREQUENCIES AND LENGTHS OF l_n

l_n (mm)	0.85	0.75	0.65	0.55
asymptotic frequency (GHz)	97.5	96.6	96.2	96.0
l_n (mm)	0.45	0.35	0.25	0.15
asymptotic frequency (GHz)	96.5	97.4	98.7	100.7

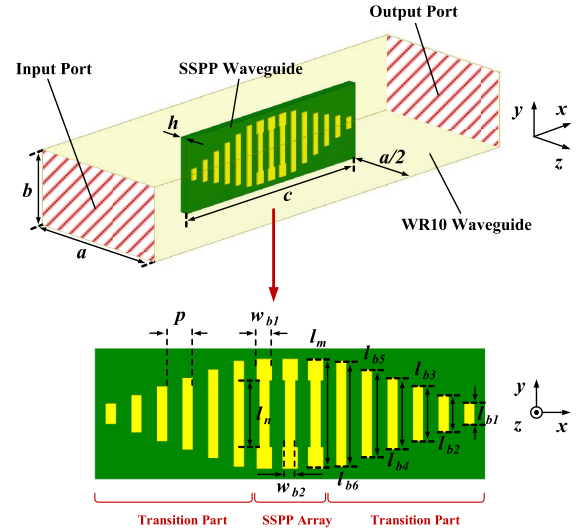


Fig. 9. Millimeter-wave E-plane waveguide BPF based on stepped-impedance SSPPs.

bandwidths of upper and lower stopbands are both 61 GHz. The simulated $|S_{21}|$ curves of the proposed BPF with different values of w_{b1} are presented in Fig. 10(b). It can be clearly noticed that the increase of w_{b1} will decrease the upper cutoff frequency from 103 to 93 GHz for the proposed BPF, which agrees well with the relationships between asymptotic frequencies and parameter w_{b1} in Fig. 8.

For demonstration, the transmission characteristics and electric field distributions of the proposed BPF are shown in Fig. 11. Three operating frequency points of the electric field

TABLE III
DIMENSIONS OF MILLIMETER-WAVE E-PLANE
WAVEGUIDE BPF (UNIT: mm)

Parameter	l_m	l_n	l_{b1}	l_{b2}	l_{b3}
Value	1.07	0.65	0.2	0.366	0.532
Parameter	l_{b4}	l_{b5}	l_{b6}	w_{b1}	w_{b2}
Value	0.698	0.864	1.03	0.14	0.1
Parameter	p	a	b	c	h
Value	0.25	2.54	1.27	3.81	0.127

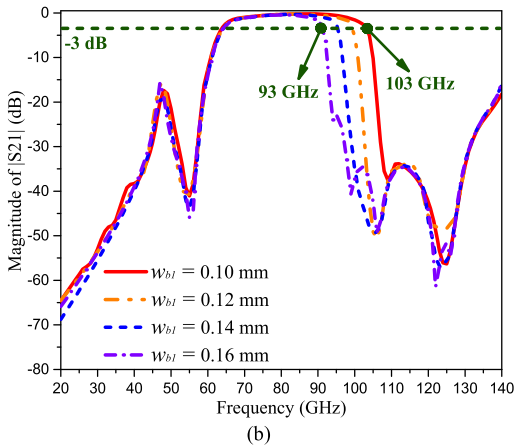
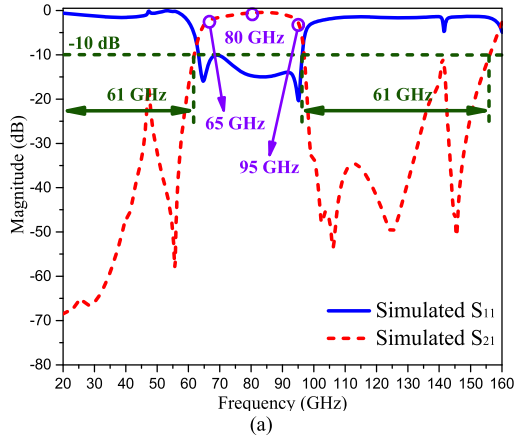


Fig. 10. (a) Simulated S-parameters of the proposed millimeter-wave E-plane waveguide BPF based on stepped-impedance SSPPs and (b) its simulated $|S_{21}|$ with different values of w_{b1} .

distributions are at 30, 80, and 120 GHz, which are selected at the below cutoff frequency of WR-10 rectangular waveguide, within the passband of the proposed BPF and above asymptotic frequency of stepped-impedance SSPP unit cell, respectively. When the proposed BPF works at 30 GHz, only few electromagnetic waves distribute on the surface of metallic strips and cannot be transmitted to the output port of the proposed BPF in Fig. 11(a), which is caused by the high-pass characteristics of WR-10 rectangular waveguide. Within the passband, the electromagnetic wave can propagate through the SSPP waveguide and realized effective mode conversion, as shown in Fig. 11(b). Due to the observation frequency

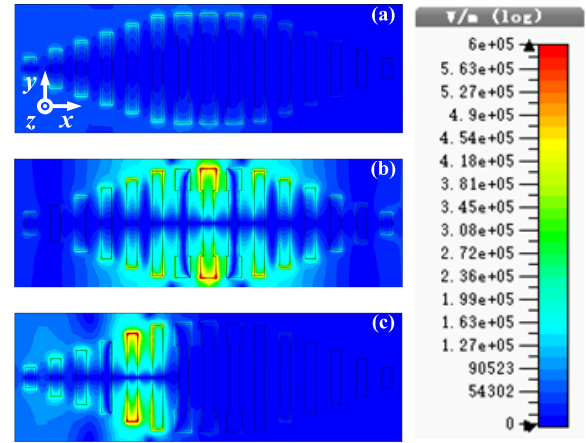


Fig. 11. Electric field distributions of the proposed millimeter-wave E-plane waveguide BPF based on stepped-impedance SSPPs at (a) 30, (b) 80, and (c) 120 GHz.

point 120 GHz located far away from the fundamental mode of stepped-impedance SSPPs, the electromagnetic wave fed by WR-10 rectangular waveguide gradually disappears and cannot propagate through the SSPP waveguide, as illustrated in Fig. 11(c).

B. Millimeter-Wave E-Plane Waveguide BPF Based on Grounded SSPPs

In this section, a grounded SSPP unit cell, which consists of two symmetrically metallic strips grounded to the walls of the rectangular waveguide, is proposed, as shown in Fig. 12(a) (inset). The initial dimensions of the proposed SSPP unit cell are $l_c = 0.585$ mm, $w_c = 0.1$ mm, and $p = 0.235$ mm. To apply the proposed SSPP unit cell for the design of millimeter-wave E-plane waveguide BPF, the dispersive characteristics of grounded SSPP unit cell are also investigated first. The dispersion curves with different parameters of l_c , w_c , and p are simulated.

As shown in Fig. 12, the variation of l_c has more obvious influence on the distribution of asymptotic frequency than that of other two parameters for the proposed SSPP unit cell. The asymptotic frequency can be adjusted from 103 to 93 GHz, as l_c is tuned from 0.540 to 0.585 mm. The variation of l_c does not increase the occupied area of SSPP waveguide. Besides, the asymptotic frequencies of dispersion curves in Fig. 12(b) are almost unchanged near 94.0 GHz with the change of w_c from 0.02 to 0.14 mm. The maximum feasible value of w_c is only 0.135 mm for the limitation of fabricated resolution and the fixed size in the y -direction of WR-10 rectangular waveguide, which unavoidably limits the adjustment ability of grounded SSPP unit cell. Therefore, if the proposed SSPP unit cell is applied for the design of millimeter-wave E-plane waveguide BPF, the parameter l_c can be a proper option for the adjustment of upper cutoff frequency of BPF.

Based on the aforementioned analysis, a millimeter-wave E-plane waveguide BPF based on grounded SSPPs is proposed. Its layout along with the top view of the inserted substrate is shown in Fig. 13. All dimensions of the proposed

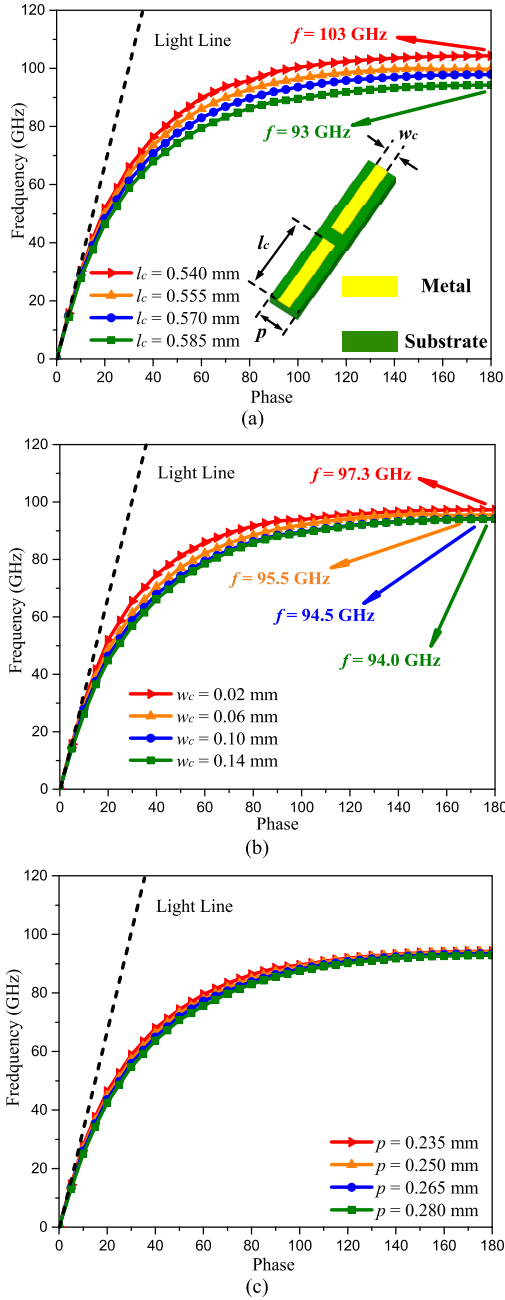


Fig. 12. Dispersion curves of the grounded SSPP unit cell with different values of (a) l_c , (b) w_c , and (c) p .

BPF are tabulated in Table IV. For this case, the y -directional lengths of metallic strips of gradient transition parts are set as follows:

$$l_{cn} = 0.084375(n - 1) + 0.1125, \quad n = 1, 2, \dots, 6. \quad (4)$$

Fig. 14(a) displays the simulated S-parameters of the proposed BPF, and the simulation of $|S_{21}|$ with different values of l_c is displayed in Fig. 14(b). It can be seen in Fig. 14(a) that the proposed BPF has a passband from 67 to 100 GHz with a 3-dB fractional bandwidth of 39.5%, and its simulated center frequency is at 83.5 GHz with an insertion loss of 0.35 dB. The proposed BPF also has wide out-of-band rejection (referring to -10 dB), whose simulated bandwidths of upper and lower

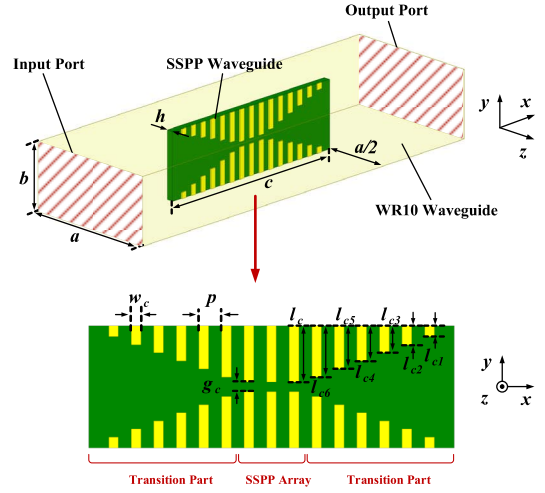


Fig. 13. Millimeter-wave E-plane waveguide BPF based on grounded SSPPs.

TABLE IV
DIMENSIONS OF MILLIMETER-WAVE E-PLANE
WAVEGUIDE BPF (UNIT: mm)

Parameter	l_c	l_{c1}	l_{c2}	l_{c3}	l_{c4}
Value	0.555	0.1125	0.197	0.281	0.366
Parameter	l_{c5}	l_{c6}	w_c	g_c	a
Value	0.45	0.534	0.1	0.1	2.54
Parameter	b	c	h		
Value	1.27	3.81	0.127		

stopbands are 56 and 65 GHz, respectively. As l_c increases from 0.54 to 0.585 mm, the upper cutoff frequency will be reduced from 103 to 93 GHz for the proposed BPF, which agrees well with the relationships between asymptotic frequencies and parameter l_c in Fig. 12(a).

To observe the transmission characteristics, Fig. 15 illustrates the electric field distributions at the operating frequencies of 30, 80, and 120 GHz, which are located at the lower stopband, passband, and upper stopband of the proposed BPF, respectively. The electromagnetic wave cannot propagate through the SSPP waveguide in Fig. 15(a) when its working frequency (30 GHz) is smaller than the cutoff frequency of WR-10 rectangular waveguide. It can be observed in Fig. 15(b) that only the electromagnetic wave in the passband can propagate through the SSPP waveguide. Besides, the electric field distribution of y - o - z cross section in Fig. 15(b) indicates that the propagation of electromagnetic wave can be effectively confined on the surface of SSPP waveguide. When the proposed BPF is operated at 120 GHz in Fig. 15(c), the electromagnetic wave can be effectively blocked and cannot propagate through the SSPP waveguide from input port to output port.

IV. FABRICATION AND MEASUREMENT

To verify the feasibility of BPF designs, the millimeter-wave E-plane waveguide BPFs based on uniform, stepped-impedance, and grounded SSPPs are fabricated and measured,

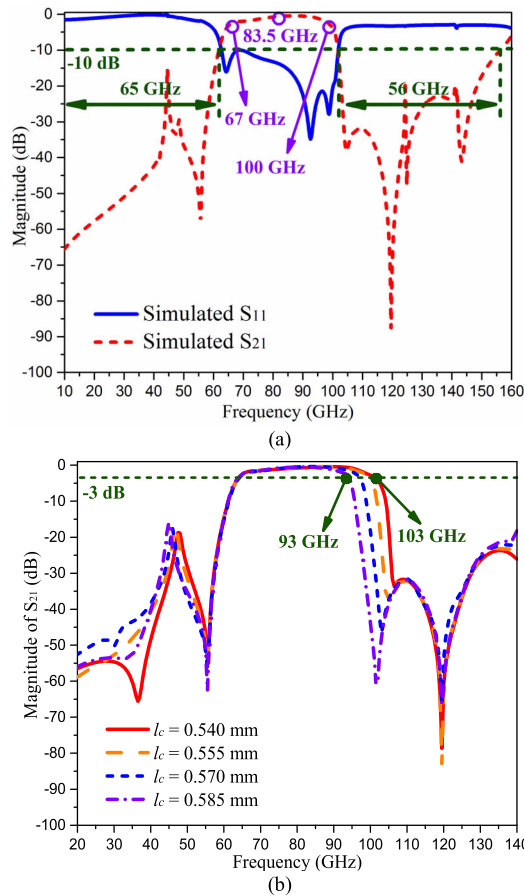


Fig. 14. (a) Simulated S-parameters of the proposed millimeter-wave E-plane waveguide BPF based on grounded SSPPs and (b) its simulated $|S_{21}|$ with different values of l_c .

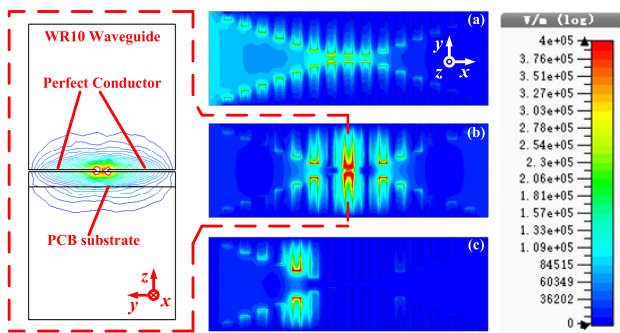


Fig. 15. Electric field distributions of the proposed BPF at (a) 30, (b) 80, and (c) 120 GHz.

respectively. The measured setup of these fabricated BPFs is displayed in Fig. 16(a) and (b). The inner profile of fabricated WR-10 rectangular waveguide is illustrated in Fig. 16(c) for observing the structures of fabricated BPFs. The proposed SSPP waveguides are placed in the slots of bottom cavity, and the total length of waveguide is 20 mm for the connection with W-band extender module and vector network analyzer Ceyear AV3672E.

Although the measurements of millimeter-wave E-plane waveguide BPFs are not supported in the whole frequency

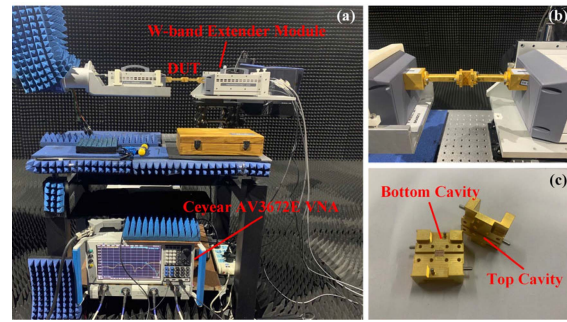


Fig. 16. (a) Measurement platform, (b) zoomed-in view of the device under test (DUT), and (c) inner profile of the fabricated WR-10 waveguide.

TABLE V
PERFORMANCE COMPARISONS WITH PREVIOUS W-BAND BPFs

	CF (GHz)	FBW (%)	IL (dB)	RL (dB)	SF	Size (mm ³)	Tech.
[4]	93	3.4	4.3	>13.5	1.67	4.20×2.20×0.07	70μm GaAs
[10]	80	3.75	3.89	>13	1.5	5.90×4.10×0.508	SIW
[20]	91.3	5.3	1.6	>18	2.02	3.81×2.54×1.27	E-plane Waveguide
[21]	98	6.9	0.6	>15	2.2	2.60×2.54×1.27	E-plane Waveguide
[37]	97	6.5	1.02	>14	1.36	3.21×2.54×1.27	E-plane Waveguide
[38]	88.55	3.6	1.15	>18	2.06	3.21×2.54×1.27	E-plane Waveguide
[39]	82.7	6	0.4	>8	1.3	20.8×2.54×1.27	E-plane Waveguide
[40]	88.47	9.7	1.1	>15	1.63	12.3×2.54×1.27	SU-8
[41]	88.34	12.1	1.94	>18	1.26	7.94×2.54×1.27	Waveguide
This Work1	85	44.7	0.58	>10	1.02	3.81×2.54×1.27	E-plane Waveguide
This Work2	80	37.3	0.4	>10	1.19	3.81×2.54×1.27	
This Work3	83	44.7	0.35	>10	1.25	3.81×2.54×1.27	

*CF: center frequency. FBW_{3dB}: 3-dB fractional bandwidth. IL and RL mean insertion loss and return loss within the passband, respectively. SF: shape factor, SF = FBW_{20dB}/FBW_{3dB}, where FBW_{20dB} means the 20-dB fractional bandwidth.

region due to the measured limitation of frequency extender module, the fabricated BPFs are tested in the entire W-band (75–110 GHz). The measured S-parameters along with the corresponding photographs of these three fabricated BPFs are displayed in Fig. 17.

Good agreement between simulated and measured results of the fabricated BPFs can be clearly observed in Fig. 17. It can be seen that all measured reflection coefficients (S_{11}) of fabricated BPFs are below -10 dB, and the measured minimum insertion losses are 0.58, 0.4, and 0.35 dB, respectively. All three fabricated BPFs have flat passbands and sharp roll-off skirts. The slight deviations between simulated and measured results of the proposed BPFs are mainly caused by the inaccuracies of manufacturing and assembling. Based on

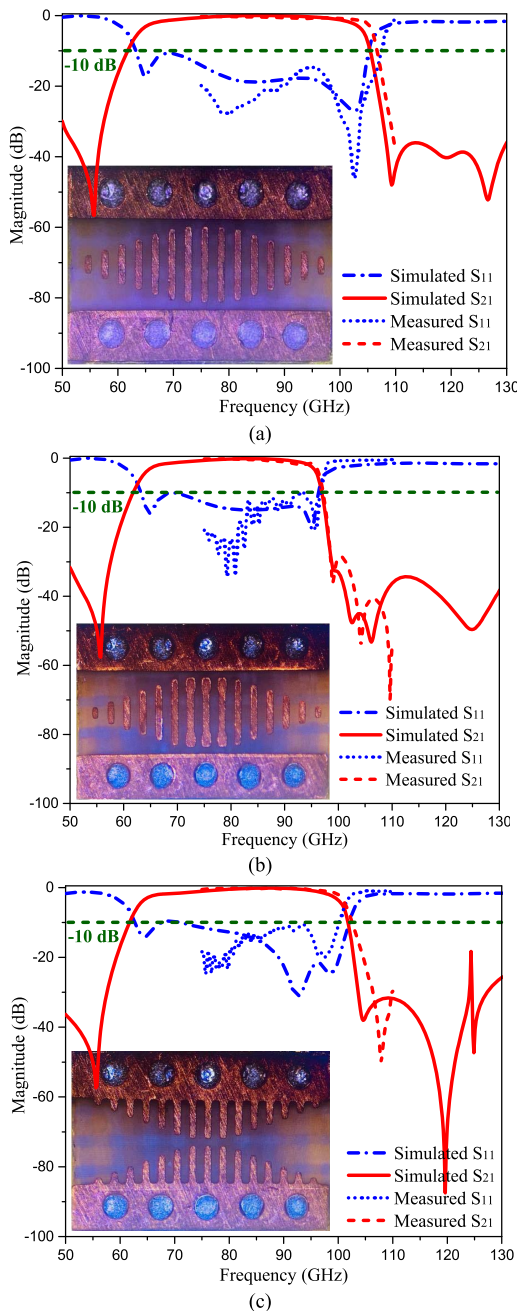


Fig. 17. Simulated and measured results of the E-plane waveguide BPFs based on (a) uniform SSPPs, (b) stepped-impedance SSPPs, and (c) grounded SSPPs.

the measured results, it is verified that all of these fabricated BPFs possess good filtering performance and wide out-of-band rejection level.

Table V tabulates the characteristic comparisons of the proposed BPFs with some previously reported works. As can be observed, comparing with the works presented in [20], [21], [37], [38], and [39], our designs use the same technology for implementation and operate at W-band, but achieve better insertion losses and shape factors.

V. CONCLUSION

Novel millimeter-wave E-plane waveguide BPFs based on three different SSPPs are presented. The bandwidths and

upper cutoff frequencies of the proposed BPFs can be flexibly adjusted by controlling the asymptotic frequencies of SSPP unit cells. Reasonable agreement between measured and simulated results indicates that the design method of the proposed E-plane waveguide BPFs is very attractive for the applications in millimeter-wave wireless communication systems.

REFERENCES

- [1] D. M. Kang, J. Y. Hong, J. Y. Shim, J. H. Lee, H. S. Yoon, and K. H. Lee, "A 77 GHz automotive radar MMIC chip set fabricated by a 0.15 μm MHEMT technology," in *IEEE MTT-S Int. Microw. Symp. Dig.*, Jun. 2005, pp. 2111–2114.
- [2] C. Riva, C. Capsoni, L. Luini, M. Luccini, R. Nebuloni, and A. Martellucci, "The challenge of using the W band in satellite communication," *Int. J. Satell. Commun. Netw.*, vol. 32, no. 3, pp. 187–200, May 2014.
- [3] L. Yujiri, "Passive millimeter wave imaging," in *IEEE MTT-S Int. Microw. Symp. Dig.*, Jun. 2006, pp. 98–101.
- [4] Y. Xiao, P. Shan, Y. Zhao, H. Sun, and F. Yang, "Design of a W-band GaAs-based SIW chip filter using higher order mode resonances," *IEEE Microw. Wireless Compon. Lett.*, vol. 29, no. 2, pp. 104–106, Feb. 2019.
- [5] Y. Yang, H. Liu, Z. J. Hou, X. Zhu, E. Dutkiewicz, and Q. Xue, "Compact on-chip bandpass filter with improved in-band flatness and stopband attenuation in 0.13- μm (Bi)-CMOS technology," *IEEE Electron Device Lett.*, vol. 38, no. 10, pp. 1359–1362, Oct. 2017.
- [6] H.-R. Chuang, L.-K. Yeh, P.-C. Kuo, K.-H. Tsai, and H.-L. Yue, "A 60-GHz millimeter-wave CMOS integrated on-chip antenna and bandpass filter," *IEEE Trans. Electron Devices*, vol. 58, no. 7, pp. 1837–1845, Jul. 2011.
- [7] K.-D. Xu, Y.-J. Guo, Y. Liu, X. Deng, Q. Chen, and Z. Ma, "60-GHz compact dual-mode on-chip bandpass filter using GaAs technology," *IEEE Electron Device Lett.*, vol. 42, no. 8, pp. 1120–1123, Aug. 2021.
- [8] A. S. El-Hameed, A. Barakat, A. B. Abdel-Rahman, A. Allam, and R. K. Pokharel, "Ultracompact 60-GHz CMOS BPF employing broadside-coupled open-loop resonators," *IEEE Microw. Wireless Compon. Lett.*, vol. 27, no. 9, pp. 818–820, Sep. 2017.
- [9] S. W. Wong, K. Wang, Z.-N. Chen, and Q.-X. Chu, "Design of millimeter-wave bandpass filter using electric coupling of substrate integrated waveguide (SIW)," *IEEE Microw. Wireless Compon. Lett.*, vol. 24, no. 1, pp. 26–28, Jan. 2014.
- [10] Z. C. Hao, W. Q. Ding, and W. Hong, "Developing low-cost W-band SIW bandpass filters using the commercially available printed-circuit-board technology," *IEEE Trans. Microw. Theory Techn.*, vol. 64, no. 6, pp. 1775–1786, Jun. 2016.
- [11] J. A. Martinez, J. J. de Dios, A. Belenguer, H. Esteban, and V. E. Boria, "Integration of a very high quality factor filter in empty substrate-integrated waveguide at Q-band," *IEEE Microw. Wireless Compon. Lett.*, vol. 28, no. 6, pp. 503–505, Jun. 2018.
- [12] D. Stephens, P. R. Young, and I. D. Robertson, "Millimeter-wave substrate integrated waveguides and filters in photoimageable thick-film technology," *IEEE Trans. Microw. Theory Techn.*, vol. 53, no. 12, pp. 3832–3838, Dec. 2005.
- [13] S. W. Wong, R. S. Chen, K. Wang, Z.-N. Chen, and Q.-X. Chu, "U-shape slots structure on substrate integrated waveguide for 40-GHz bandpass filter using LTCC technology," *IEEE Trans. Compon., Packag., Manuf. Technol.*, vol. 5, no. 1, pp. 128–134, Jan. 2015.
- [14] T. M. Shen, C. F. Chen, T. Y. Huang, and R. B. Wu, "Design of vertically stacked waveguide filters in LTCC," *IEEE Trans. Microw. Theory Techn.*, vol. 55, no. 8, pp. 1771–1779, Aug. 2007.
- [15] M. T. Sebastian and H. Jantunen, "Low loss dielectric materials for LTCC applications: A review," *Int. Mater. Rev.*, vol. 52, no. 2, pp. 57–99, 2008.
- [16] K. Wu, H. Zhang, Y. Chen, Q. Luo, and K. Xu, "All-silicon microdisplay using efficient hot-carrier electroluminescence in standard 0.18 μm CMOS technology," *IEEE Electron Device Lett.*, vol. 42, no. 4, pp. 541–544, Apr. 2021.
- [17] K. Xu, "Integrated silicon directly modulated light source using p-well in standard CMOS technology," *IEEE Sensors J.*, vol. 16, no. 16, pp. 6184–6191, Aug. 2016.
- [18] K. Xu, "Monolithically integrated Si gate-controlled light-emitting device: Science and properties," *J. Opt.*, vol. 20, no. 2, Jan. 2018, Art. no. 024014.

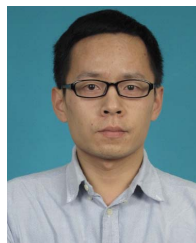
- [19] K. Xu, "Silicon electro-optic micro-modulator fabricated in standard CMOS technology as components for all silicon monolithic integrated optoelectronic systems," *J. Micromech. Microeng.*, vol. 31, no. 5, May 2021, Art. no. 054001.
- [20] K.-D. Xu, S. Xia, Y.-J. Guo, J. Cui, A. Zhang, and Q. Chen, "W-band E-plane waveguide bandpass filter based on meander ring resonator," *IEEE Microw. Wireless Compon. Lett.*, vol. 31, no. 12, pp. 1267–1270, Dec. 2021.
- [21] Z. Y. Huang, Y. Jiang, J. J. Huang, W. D. Hu, and N. C. Yuan, "Flexible design of W-band bandpass filter with multiple transmission zeros," *Microw. Opt. Technol. Lett.*, vol. 63, pp. 2355–2358, Jun. 2021.
- [22] J. Y. Jin, X. Q. Lin, Y. Jiang, and Q. Xue, "A novel compact E-plane waveguide filter with multiple transmission zeroes," *IEEE Trans. Microw. Theory Techn.*, vol. 63, no. 10, pp. 3374–3380, Oct. 2015.
- [23] H. Raether, "Surface plasmons on gratings," in *Surface Plasmons on Smooth and Rough Surfaces and on Gratings* (Springer Tracts Modern Physics), vol. 111. Berlin, Germany: Springer, 1988, pp. 91–116.
- [24] J. B. Pendry, L. Martín-Moreno, and F. J. Garcia-Vidal, "Mimicking surface plasmons with structured surfaces," *Science*, vol. 305, pp. 847–848, Aug. 2004.
- [25] X. Liu, Y. Feng, B. Zhu, J. Zhao, and T. Jiang, "High-order modes of spoof surface plasmonic wave transmission on thin metal film structure," *Opt. Exp.*, vol. 21, no. 25, pp. 31155–31165, 2013.
- [26] S. Lu, K.-D. Xu, Y.-J. Guo, and Q. Chen, "Compact spoof surface plasmon polariton waveguides with simple configurations and good performance," *IEEE Trans. Plasma Sci.*, vol. 49, no. 12, pp. 3786–3792, Dec. 2021.
- [27] J. Li, K.-D. Xu, J. Shi, Y.-J. Guo, and A. Zhang, "Spoof surface plasmon polariton waveguide with switchable notched band," *IEEE Photon. Technol. Lett.*, vol. 33, no. 20, pp. 1147–1150, Oct. 15, 2021.
- [28] Y. Liu, K.-D. Xu, Y.-J. Guo, and Q. Chen, "High-order mode application of spoof surface plasmon polaritons in bandpass filter design," *IEEE Photon. Technol. Lett.*, vol. 33, no. 7, pp. 362–365, Apr. 1, 2021.
- [29] C. Han, Z. H. Wang, Y. Y. Chu, X. D. Zhao, and X. R. Zhang, "Compact flexible multifrequency splitter based on plasmonic graded metallic grating arc waveguide," *Opt. Lett.*, vol. 43, no. 8, pp. 1898–1901, 2018.
- [30] D.-F. Guan, P. You, Q. Zhang, Z.-H. Lu, S.-W. Yong, and K. Xiao, "A wide-angle and circularly polarized beam-scanning antenna based on microstrip spoof surface plasmon polariton transmission line," *IEEE Antennas Wireless Propag. Lett.*, vol. 16, pp. 2538–2541, 2017.
- [31] Y. Wu, M. Li, G. Yan, L. Deng, Y. Liu, and Z. Ghassemloooy, "Single-conductor co-planar quasi-symmetry unequal power divider based on spoof surface plasmon polaritons of bow-tie cells," *AIP Adv.*, vol. 6, no. 10, Oct. 2016, Art. no. 105110.
- [32] H. F. Ma, X. Shen, Q. Cheng, W. X. Jiang, and T. J. Cui, "Broadband and high-efficiency conversion from guided waves to spoof surface plasmon polaritons," *Laser Photon. Rev.*, vol. 8, no. 1, pp. 146–151, 2014.
- [33] M. Wang, H. F. Ma, W. X. Tang, H. C. Zhang, Z. X. Wang, and T. J. Cui, "Programmable controls of multiple modes of spoof surface plasmon polaritons to reach reconfigurable plasmonic devices," *Adv. Mater. Technol.*, vol. 4, no. 3, Jan. 2019, Art. no. 1800603.
- [34] M. Wang, S. Sun, H. F. Ma, and T. J. Cui, "Supercompact and ultrawideband surface plasmonic bandpass filter," *IEEE Trans. Microw. Theory Techn.*, vol. 68, no. 2, pp. 732–740, Feb. 2020.
- [35] Z. W. Cheng, H. F. Ma, M. Wang, and T. J. Cui, "Dual-beam leaky-wave radiations with independent controls of amplitude, angle, and polarization based on SSPP waveguide," *Adv. Photon. Res.*, vol. 3, no. 5, May 2022, Art. no. 2100313.
- [36] Y. Liu and K.-D. Xu, "W-band waveguide bandpass filters based on spoof surface plasmon polaritons," in *Proc. IEEE Int. Workshop Electromagn., Appl. Student Innov. Competition (iWEM)*, Nov. 2021, pp. 1–3, doi: 10.1109/iWEM53379.2021.9790540.
- [37] Y. Jiang, K. D. Xu, and Z. Y. Huang, "Compact W-band E-plane waveguide filter with high selectivity," *J. Infr. Millim., Terahertz Waves*, vol. 43, pp. 294–302, Apr. 2022, doi: 10.1007/s10762-022-00851-9.
- [38] Y. Jiang *et al.*, "W-band E-plane waveguide filter using compact beeline resonator," *IEEE Microw. Wireless Compon. Lett.*, vol. 32, no. 4, pp. 289–292, Apr. 2022.
- [39] M. Zhao, Z. He, Y. Fan, and Y. Zhang, "A W-band wideband E-plane type waveguide bandpass filter," in *Proc. 8th U.K., Eur., China Millim. Waves THz Technol. Workshop (UCMMT)*, Cardiff, U.K., Sep. 2015, pp. 14–15.

- [40] X. Shang, M. Ke, Y. Wang, and M. Lancaster, "Micromachined W-band waveguide and filter with two embedded H-plane bends," *IET Microw. Antennas Propag.*, vol. 5, no. 3, pp. 334–339, Feb. 2011.
- [41] M. Salek *et al.*, "W-band waveguide bandpass filters fabricated by micro laser sintering," *IEEE Trans. Circuits Syst. II, Exp. Briefs*, vol. 66, no. 1, pp. 61–65, Jan. 2019.



Yiqun Liu (Student Member, IEEE) received the B.S. and M.S. degrees from Xi'an Jiaotong University, Xi'an, China, in 2015 and 2019, respectively, where he is currently pursuing the Ph.D. degree at the School of Information and Communication Engineering.

His research interests include microwave device and circuit design.



Kai-Da Xu (Senior Member, IEEE) received the B.E. and Ph.D. degrees in electromagnetic field and microwave technology from the University of Electronic Science and Technology of China (UESTC), Chengdu, China, in 2009 and 2015, respectively.

From 2012 to 2014, he was a Visiting Researcher with the Department of Electrical and Computer Engineering, Duke University, Durham, NC, USA, supported by the China Scholarship Council. In 2015, he joined the Department of Electronic Science, Xiamen University, Xiamen, China, as an Assistant Professor. From 2016 to 2017, he was a Post-Doctoral Fellow with the State Key Laboratory of Millimeter Waves, City University of Hong Kong, Hong Kong. From 2018 to 2019, he was an Honorary Fellow with the Department of Electrical and Computer Engineering, University of Wisconsin–Madison, Madison, WI, USA. He was successfully selected into the Youth Talent Support Program of Xi'an Jiaotong University (XJTU), Xi'an, China, in 2019, where he joined the School of Information and Communications Engineering in 2020. He has authored and coauthored over 140 papers in peer-reviewed journals and over 40 papers in conference proceedings. His current research interests include RF/microwave, millimeter-wave (mm-wave)/THz devices, and antenna arrays.

Dr. Xu was the Japan Society for the Promotion of Science (JSPS) Fellow with the Department of Communications Engineering, Graduate School of Engineering, Tohoku University, from 2019 to 2021. He has been serving as an Editorial Board Member for both the *AEU-International Journal of Electronics and Communications* and *MDPI Electronics*. He received a fellowship from the JSPS. He received the UESTC Outstanding Graduate Awards in 2009 and 2015, respectively. He was a recipient of the National Graduate Student Scholarship in 2012, 2013, and 2014 from the Ministry of Education, China. Since 2017, he has been serving as an Associate Editor for the *IEEE ACCESS* and *Electronics Letters*.



Jianxing Li (Member, IEEE) received the B.S. degree in information and communications engineering and the M.S. and Ph.D. degrees in electromagnetic field and microwave techniques from Xi'an Jiaotong University, Xi'an, China, in 2008, 2011, and 2016, respectively.

From 2014 to 2016, he was a Visiting Researcher with the Department of Electrical and Computer Engineering, Duke University, Durham, NC, USA. He is currently an Associate Professor with Xi'an Jiaotong University. His research interests include

microwave and millimeter-wave (mm-wave) circuits and antennas, wireless power transfer, and multifunctional mm-wave antennas.



Ying-Jiang Guo (Member, IEEE) received the B.E. degree in electronic engineering from Sichuan University, Chengdu, China, in 2008, and the Ph.D. degree in electronic engineering from the University of Electronic Science and Technology of China, Chengdu, in 2018.

From 2011 to 2013, he was with Huawei Technologies Company Ltd., Shenzhen, China, where he was involved in the research of 5G communication prototype design. From 2013 to 2014, he was with Sichuan Normal University, Chengdu, where he was a Lecturer. From 2018 to 2021, he was with the Microsystem and Terahertz Research Center, China Academy of Engineering Physics, Mianyang, China, as an Assistant Research Fellow, where he was involved in focusing on the terahertz integrated circuits and communication technologies. Since 2021, he has been with Allwinner Technology Company Ltd., Zhuhai, China, as a Senior RF/Analog IC Engineer and an Associate Research Fellow. He has authored or coauthored over 50 journal and conference papers. He holds over five patents in wireless communication. His research interests include the RF/microwave/millimeter-wave (mm-wave) circuits, THz modules/antennas, and systems in package.



Anxue Zhang (Member, IEEE) received the B.S. degree in electrical engineering from Henan Normal University, Xinxiang, China, in 1996, and the M.S. and Ph.D. degrees in electromagnetic and microwave engineering from Xi'an Jiaotong University, Xi'an, China, in 1999 and 2003, respectively.

He is currently a Professor with Xi'an Jiaotong University. His research interests include antenna and electromagnetic wave propagation, RF and microwave circuit design, and metamaterials.



Qiang Chen (Senior Member, IEEE) received the B.E. degree from Xidian University, Xi'an, China, in 1986, and the M.E. and D.E. degrees from Tohoku University, Sendai, Japan, in 1991 and 1994, respectively.

He is currently the Chair Professor of the Electromagnetic Engineering Laboratory, Department of Communications Engineering, School of Engineering, Tohoku University. His research interests include antennas, microwave and millimeter wave, antenna measurement, and computational

electromagnetics.

Dr. Chen is a Fellow of the Institute of Electronics, Information and Communication Engineers (IEICE). He received the Best Paper Award and the Zenichi Kiyasu Award in 2009 from the IEICE. He served as the Chair of the IEICE Technical Committee on Photonics-Applied Electromagnetic Measurement from 2012 to 2014, the Chair of the IEICE Technical Committee on Wireless Power Transfer from 2016 to 2018, and the Chair of the Tokyo Chapter of the IEEE Antennas and Propagation Society from 2017 to 2018. He is the Chair of the IEICE Technical Committee on Antennas and Propagation.